

CONTROL OF LASERT RADIATION PARAMETERS

https://doi.org/10.1070/QEL17652

Electromagnetically induced transparency under phase modulation of interacting radiations

O.M. Parshkov

Abstract. **We report the results of an analytical and numerical analysis of the evolution of nanosecond probe pulses in the case of electromagnetically induced transparency in the Λ-scheme of degenerate quantum transitions. It is assumed that the probe and control fields at the active medium input are elliptically polarised, and one of them is phase modulated. It is shown analytically that probe radiation in a medium is the sum of two normal modes propagating independently of each other. Because the group velocities of normal mode pulses are different, a single probe pulse entering the medium decays inside the medium into separate pulses, each of which transfers the energy of one of the normal modes. Numerical simulations have shown that with a sufficiently large phase modulation, normal modes, whose intensity on the input surface is described by a bell-shaped curve, turn into trains of subpulses in the medium. Phase modulation of the input field has practically no effect on the group propagation velocities of normal modes, but it reduces the transparency of the medium for probe radiation.**

Keywords: *electromagnetically induced transparency, phase modulation, normal modes.*

1. Introduction

Resonant action of two coherent laser fields on two quantum transitions with a common energy level [1] leads to a number of effects interesting from the theoretical and practical points of view. Among them, a special place is occupied by the phenomenon of electromagnetically induced transparency (EIT) [2–4]. The use of EIT opens up new opportunities for the development of optical memory [3], quantum communications [3, 5, 6], quantum information systems [2–4], devices for high-precision measurement of magnetic fields [7], and chronometry devices [8]. The EIT phenomenon underlies the methods of generating large optical nonlinearities [4, 9] and amplifying radiation without population inversion of quantum transitions [10]. Research is underway of the features of the EIT manifestation in new situations, for example, in strongly correlated quantum gases [11], in the case of radio waves [12], on impurities in photonic crystals [13], near a nanofiber [14], and in the presence of an angular orbital momentum in the probe field [15].

In the case of degeneracy of the energy levels of quantum transitions, the EIT phenomenon acquires new features associated with the polarisation states of the interacting fields. For example, the authors of Refs [16, 17] studied theoretically and experimentally the rotation of the polarisation plane of the probe field with a change in the control radiation intensity. The results of theoretical and experimental studies of the effect of a constant magnetic field on the evolution of the circular components of the probe radiation are presented in [18, 19]. Yoon et al. [20] studied experimentally and theoretically the circular birefringence of the probe field accompanying the EIT phenomenon. Kis et al. [21] predicted theoretically the possibility of propagation of a probe field in the form of two modes with different polarisation states in the stationary EIT regime.

In the above works, the theory was based on the adiabatic approximation [22, 23], which is applicable to the description of pulses of sufficiently long duration [24]. In our paper [25], we considered theoretically, without using the adiabatic approximation, the pulsed regime of the EIT phenomenon in the Λ-scheme formed by the levels $^3P_0$, $^3P_2$, $^3P_1^0$ of the ^{208}Pb isotope, in which EIT of circularly polarised laser fields was experimentally observed [26, 27]. It was shown in [25] that the probe field inside the medium is the sum of normal modes, the pulses of which propagate with different group velocities. The theory developed in [25] had a limited field of application due to the assumption that, at the resonant medium input, pulses of interacting radiations do not exhibit phase modulation (PM). This paper presents the results of an analytical and numerical study of the features of the EIT phenomenon in the presence of phase modulation of one of the interacting fields on the input surface of a resonant medium.

2. Initial equations

The Λ-scheme in question is formed by simple degenerate lower ($^3P_0$), fivefold degenerate middle ($^3P_2$), and triply degenerate upper ($^3P_1^0$) levels of the ^{208}Pb atom. We introduce an orthonormal basis ϕ_k ($k = 1, 2, \ldots, 9$) of the common eigenfunctions of the operators of energy, square and projection of the angular momentum on the z axis of the ^{208}Pb isotope, corresponding to the lower ($k = 1$, $M = 0$), upper ($k = 2, 3, 4$; $M = -1, 0, 1$) and middle ($k = 5, 6, \ldots, 9$; $M = -2, -1, 0, 1, 2$) levels. Let D_1 and D_2 be the reduced electric dipole moments of the $^3P_0 \rightarrow {}^3P_1^0$ and $^3P_2 \rightarrow {}^3P_1^0$ transitions, respectively, and ω_1 and ω_2 ($\omega_1 > \omega_2$) be the frequencies of these transitions for an atom at rest. We describe the inhomogeneous broadening of spectral lines by a Doppler contour with the parameter T_1. The width Δ_1 of the inhomogeneously broadened $^3P_0 \rightarrow {}^3P_1^0$ transition line determined from the e^{-1} level is given by the ratio $\Delta_1 = 2/T_1$.

We define the strength $\boldsymbol{E}$ of the total electric field acting on the medium in the form

O.M. Parshkov Yuri Gagarin State Technical University of Saratov, ul. Polytekhnicheskaya 77, 410054 Saratov, Russia;
e-mail: Oparshkov@mail.ru

Received 21 September 2021
Kvantovaya Elektronika **51** (12) 1127–1134 (2021)
Translated by I.A. Ulitkin

$$\boldsymbol{E} = \boldsymbol{E}_1 + \boldsymbol{E}_2,\ \ \boldsymbol{E}_l = \mu_l[\boldsymbol{e}_x E_{xl}\cos(\omega_l t - k_l z + \delta_{xl})$$

$$+ \boldsymbol{e}_y E_{yl}\cos(\omega_l t - k_l z + \delta_{yl})],\ \ l = 1, 2. \qquad (1)$$

Here $\boldsymbol{E}_l$ and ω_l are the electric field strength and the carrier frequency of the probe (l = 1) and control (l = 2) fields; $\mu_l = \hbar\sqrt{2l+1}/(|D_l|T_1)$; $\boldsymbol{e}_x$ and $\boldsymbol{e}_y$ are unit vectors along the x and y axes; E_{xl} and E_{yl} are nonnegative real amplitudes; δ_{xl} and δ_{yl} ($-\pi \leqslant \delta_{xl}, \delta_{yl} \leqslant \pi$) are the phase additions of the x- and y-components of the probe (l = 1) and control (l = 2) fields; and $k_l = \omega_l/c$. Following [28], we introduce f_l and g_l, which denote the amplitudes of the left- and right-hand circular components of the probe (l = 1) and control (l = 2) fields. Let us define the normalised independent variables

$$s = z/z_0,\ \ w = (t - z/c)/T_1,$$

where $z_0 = 3\hbar c/(2\pi N|D_1|^2 T_1\omega_1)$ and N is the concentration of atoms. We introduce $\varepsilon_1 = T_1(\omega_1 - \omega_1')$, and $\varepsilon_2 = \omega_2\varepsilon_1/\omega_1$, where ω_1' is the frequency of the $^3P_0 \rightarrow {}^3P_1^0$ transition of a moving atom, and the constant $\xi = 0.6(\omega_2/\omega_1)|D_2/D_1|^2$. Using Maxwell's equations and the Schrödinger equation, we obtain in the first approximation of slow envelopes the system of equations:

$$\frac{\partial f_1}{\partial s} = \frac{\mathrm{i}}{\sqrt{\pi}}\int_{-\infty}^{+\infty} c_1 c_2^* \exp(-\varepsilon_1^2)\,\mathrm{d}\varepsilon_1,$$

$$\frac{\partial f_2}{\partial s} = -\frac{\mathrm{i}}{\sqrt{\pi}}\xi\int_{-\infty}^{+\infty} (c_4^* c_9 + c_2^* c_7)\exp(-\varepsilon_1^2)\,\mathrm{d}\varepsilon_1,$$

$$\frac{\partial g_1}{\partial s} = -\frac{\mathrm{i}}{\sqrt{\pi}}\int_{-\infty}^{+\infty} c_1 c_4^* \exp(-\varepsilon_1^2)\,\mathrm{d}\varepsilon_1,$$

$$\frac{\partial g_2}{\partial s} = \frac{\mathrm{i}}{\sqrt{\pi}}\xi\int_{-\infty}^{+\infty} (c_2^* c_5 + c_4^* c_7)\exp(-\varepsilon_1^2)\,\mathrm{d}\varepsilon_1,$$

$$\frac{\partial c_1}{\partial w} = -\mathrm{i}(f_1 c_2 - g_1 c_4),$$

$$\frac{\partial c_2}{\partial w} + \mathrm{i}\varepsilon_1 c_2 = -\frac{\mathrm{i}}{4}(f_1^* c_1 + g_2^* c_5 - f_2^* c_7) - \gamma c_2, \qquad (2)$$

$$\frac{\partial c_4}{\partial w} + \mathrm{i}\varepsilon_1 c_4 = \frac{\mathrm{i}}{4}(g_1^* c_1 - g_2^* c_7 + f_2^* c_9) - \gamma c_4,$$

$$\frac{\partial c_5}{\partial w} + \mathrm{i}(\varepsilon_1 - \varepsilon_2)c_5 = -\mathrm{i}g_2 c_2,$$

$$\frac{\partial c_7}{\partial w} + \mathrm{i}(\varepsilon_1 - \varepsilon_2)c_7 = \frac{\mathrm{i}}{6}(f_2 c_2 - g_2 c_4),$$

$$\frac{\partial c_9}{\partial w} + \mathrm{i}(\varepsilon_1 - \varepsilon_2)c_9 = \mathrm{i}f_2 c_4.$$

Here c_i = 1, 2, 4, 5, 7, 9 are quantities proportional to the amplitudes of the probability of the populations of the energy levels of the Λ-scheme; $\gamma = T_1/(2\tau)$; and τ is the radiative lifetime of the $^3P_1^0$ level. {A detailed derivation of equations (2) is presented in work [25].}

For the parameters of the polarisation ellipse of the probe (l = 1) and control (l = 2) fields, we use the following notations: a_l is the semi-major axis of the polarisation ellipse measured in μ_l units; α_l is the angle (in radians) between the semi-major axis and the x axis; and γ_l is the contraction parameter ($0 \leqslant \alpha_l \leqslant \pi$, $-1 \leqslant \gamma_l \leqslant 1$). Note that $|\gamma_l|$ is the ratio of the minor axis of the polarisation ellipse to its major axis, with $\gamma_l < 0$ and $\gamma_l > 0$ for the right- and left-handed elliptical polarisations, respectively. The parameters α_l and γ_l are hereinafter referred to as the polarisation characteristics of the radiation. Note that specifying a_l, α_l, and γ_l as well as of the phase additions δ_{xl} or δ_{yl} is equivalent to defining the field by formulae (1). Below, we use the dimensionless intensities I_l of the probe (l = 1) and control (l = 2) fields, measured in units of $c\mu_1^2/(8\pi)$.

The initial conditions assume that up to the instant w = 0 all the atoms of the medium are at the lower level of the Λ-scheme. Let a_{l0}, α_{l0}, γ_{l0}, and δ_{xl0} (l = 1, 2) be the values of a_l, α_l, γ_l, and δ_{xl} on the input surface (s = 0) of the resonant medium. The quantities δ_{x10} and δ_{x20} are functions of w, describing the phase-modulated radiations on this surface. We write the boundary conditions for system (3) as follows:

$$a_{10} = 0.2\,\mathrm{sech}[(w - 300)/50],\ \ \alpha_{10} = \pi/6,$$

$$\gamma_{10} = -0.5,\ \ \delta_{x1} = \delta_{x10}; \qquad (3)$$

$$a_{20} = 6.65,\ \ \alpha_{20} = 0,\ \ \gamma_{20} = -0.3,\ \ \delta_{x2} = \delta_{x20}. \qquad (4)$$

The reasons for choosing the values of the resonant medium and input radiation parameters are described in detail in [29]. Here we note that $T_1 = 1.6 \times 10^{-10}$ s, and z_0 = 0.03 cm at a temperature T_{Pb} = 950 K of saturated lead vapour. Conditions (3) describe an elliptically polarised input pulse of probe radiation with a bell-shaped envelope having a duration of 15 ns and a peak intensity of 65 W cm^{-2}; conditions (4) describe input control radiation with a constant intensity of 20 kW cm^{-2}. The intensity of the control radiation in the above-mentioned experimental works [26, 27] was approximately the same. The constancy of the value of a_{20} for the control radiation corresponds to the scheme of counterintuitive superposition of the control field, which is usually used in EIT experiments [2].

3. Normal modes in a medium

In what follows, we will assume that the probe field intensity is so low that the influence of this field on the control radiation can be neglected. Conditions (3) and (4) are in agreement with this assumption. Repeating the calculations of [25], we can show that the control radiation should propagate without absorption at the speed of light in a vacuum. Let $\alpha_{20} = 0$ and γ_{20} be a constant with $|\gamma_{20}| \neq 1$; the constant κ is given by the relations

$$\kappa = -p + \sqrt{p^2 + 1},\ \ p = 10\gamma_{20}/(1 - \gamma_{20}^2).$$

Then the representation $f_1 = f_1^{(1)} + f_1^{(2)}$, $g_1 = g_1^{(1)} + g_1^{(2)}$, where $f_1^{(1)} = \kappa g_1^{(1)}$, and $f_1^{(2)} = (1/\kappa)g_1^{(2)}$, is valid, and the sys-

tem of equations (2) simplified under the assumption of a weak probe field splits into two independent systems that determine the values of $g_1^{(k)}$ ($k = 1, 2$):

$$\begin{cases} \dfrac{\partial g_1^{(k)}}{\partial s} = \dfrac{2\mathrm{i}}{\sqrt{\pi}} \displaystyle\int_{-\infty}^{+\infty} U_k^* \exp(-\varepsilon_1^2)\,\mathrm{d}\varepsilon_1, \\ \dfrac{\partial U_k}{\partial w} + \mathrm{i}\varepsilon_1 U_k = -\dfrac{\mathrm{i}}{2} g_1^{(k)*} - \dfrac{\mathrm{i}}{4} g_{20}^*(w)\, V_k - \gamma U_k, \\ \dfrac{\partial V_k}{\partial w} + \mathrm{i}(\varepsilon_1 - \varepsilon_2)\, V_k = -\mathrm{i} g_{20} q_k U_k. \end{cases} \tag{5}$$

Here

$$g_{20} = (1/\sqrt{2}) a_{20}(1 - \gamma_{20}) \exp(\mathrm{i}\delta_{x20}),$$

$$q_1 = 1 + \kappa_2[\kappa_2 + (1/\kappa)]/6,$$

$$q_2 = 1 + \kappa_2(\kappa_2 - \kappa)/6, \;\; \kappa_2 = (1 + \gamma_{20})/(1 - \gamma_{20}).$$

The functions U_k and V_k ($k = 1, 2$) are expressed in the form of linear combinations of the quantities c_i ($i = 2, 4, 5, 7, 9$) included in system (2). Details of reducing system (2) to two independent systems (5) are presented in [25]. Note that in [25] the quantities a_{20}, α_{20}, γ_{20}, and δ_{x20} were considered constant. However, the proof that led to Eqns (5) remains valid in the case under consideration, when only the quantities α_{20} and γ_{20} are constant, while a_{20} and δ_{x20} are functions of w.

The system of equations (5) at $k = 1$, as shown in [25], describes a probe pulse with the strength $\boldsymbol{E}_1^{(1)}$ with the following characteristics of the polarisation ellipse:

$$a_1 = a_1^{(1)}, \;\; \alpha_1 = \alpha_1^{(1)} = 0, \;\; \gamma_1 = \gamma_1^{(1)}, \;\; \delta_{x1} = \delta_{x1}^{(1)},$$

where $\gamma_1^{(1)} = (\kappa - 1)/(\kappa + 1)$ is a constant, and $a_1^{(1)}$ and $\delta_{x1}^{(1)}$ may depend on w and s. This pulse will be called a parallel mode, since the main axis of its polarisation ellipse is parallel to the main axis of the polarisation ellipse of the control field.

System (5) for $k = 2$ according to [25] describes a probe pulse with the strength $\boldsymbol{E}_1^{(2)}$, for which

$$a_1 = a_1^{(2)}, \;\; \alpha_1 = \alpha_1^{(2)} = \pi/2,$$

$$\gamma_1 = \gamma_1^{(2)} = -\gamma_1^{(1)}, \;\; \delta_{x1} = \delta_{x1}^{(2)},$$

where $a_1^{(2)}$ and $\delta_{x1}^{(2)}$ may depend on w and s. This pulse is called a perpendicular mode, since the main axis of its polarisation ellipse is perpendicular to the main axis of the polarisation ellipse of the control field. If the control field is specified by formulae (4), $\gamma_1^{(1)} = 0.7417$.

The strength $\boldsymbol{E}_1$ of the probe electric field inside the medium is represented by the formula $\boldsymbol{E}_1 = \boldsymbol{E}_1^{(1)} + \boldsymbol{E}_1^{(2)}$. In what follows, we will call the field with the strength $\boldsymbol{E}_1$ the total probe field. In this case, at any points (s, w) the relation $I_1 = I_1^{(1)} + I_1^{(2)}$ is satisfied, where I_1 is the intensity of the total probe field; and $I_1^{(1)}$ and $I_1^{(2)}$ are the intensities of the parallel and perpendicular normal modes, respectively.

4. Normal modes on the input surface of a medium

To describe the evolution of normal modes in a medium using a boundary value problem, system (2) or two systems (5) require expressions that relate boundary conditions (3) for the total input probe field with the boundary conditions for normal modes from which this field is composed. In [25], such expressions were obtained for the case when the radiation on the input surface is not phase modulated. Below we present a technique for finding the boundary conditions for modes in the presence of phase modulation.

On the input surface ($s = 0$), the x- and y-components of the Jones vector $\boldsymbol{J}_{10}$ of the total probe radiation are determined by the formulae

$$J_{x10} = \mu_1 a_{10} \Omega^{(+)} \exp(\mathrm{i}\delta_{x10}),$$

$$J_{y10} = \mu_1 a_{10} \Omega^{(-)} \exp[\mathrm{i}(\delta_{x10} + \delta_1)],$$

where

$$\Omega^{(\pm)} = \sqrt{[1 + \gamma_{10}^2 \pm (1 - \gamma_{10}^2)\cos 2\alpha_{10}]/2},$$

$$\exp(\mathrm{i}\delta_1) = \frac{(1 - \gamma_{10}^2)\sin 2\alpha_{10} + 2\mathrm{i}\gamma_{10}}{\sqrt{(1 + \gamma_{10}^2)^2 - (1 - \gamma_{10}^2)^2 \cos^2 2\alpha_{10}}}.$$

The components of the Jones vector $\boldsymbol{J}_{10}^{(k)}$ of parallel ($k = 1$) and perpendicular ($k = 2$) normal modes on the input surface at $\gamma_{20} \neq 0$, which is assumed below, have the form

$$J_{x10}^{(1)} = \mu_1 a_{10}^{(1)} \exp(\mathrm{i}\delta_{x10}^{(1)}),$$

$$J_{y10}^{(1)} = \mu_1 |\gamma_1^{(1)}| a_{10}^{(1)} \exp[\mathrm{i}(\delta_{x10}^{(1)} - \mathrm{sign}(\gamma_{20})\pi/2)],$$

$$J_{x10}^{(2)} = \mu_1 |\gamma_1^{(1)}| a_{10}^{(2)} \exp(\mathrm{i}\delta_{x10}^{(2)}),$$

$$J_{y10}^{(2)} = \mu_1 a_{10}^{(2)} \exp[\mathrm{i}(\delta_{x10}^{(2)} + \mathrm{sign}(\gamma_{20})\pi/2)],$$

where $a_{10}^{(k)}$ and $\delta_{x10}^{(k)}$ are the values of the quantities $a_1^{(k)}$ and $\delta_{x1}^{(k)}$ for parallel ($k = 1$) and perpendicular ($k = 2$) normal modes at $s = 0$. Using the equality $\boldsymbol{J}_{10} = \boldsymbol{J}_{10}^{(1)} + \boldsymbol{J}_{10}^{(2)}$, we obtain

$$\begin{cases} a_{10}^{(1)} \exp(\mathrm{i}\varphi_{10}^{(1)}) + a_{10}^{(2)} \exp(\mathrm{i}\varphi_{10}^{(2)}) = a_{10}\Omega^{(+)}, \\ a_{10}^{(1)} |\gamma_1^{(1)}| \exp\left[\mathrm{i}\left(\varphi_{10}^{(1)} - \dfrac{\pi}{2}\mathrm{sign}\gamma_{20}\right)\right] \\ \quad + a_{10}^{(2)} \exp\left[\mathrm{i}\left(\varphi_{10}^{(2)} + \dfrac{\pi}{2}\mathrm{sign}\gamma_{20}\right)\right] = a_{10}\Omega^{(-)} \exp\delta_1, \end{cases} \tag{6}$$

where $\varphi_{10}^{(1)} = \delta_{x10}^{(1)} - \delta_1$ and $\varphi_{10}^{(2)} = \delta_{x10}^{(2)} - \delta_1$. The system of equations (6) is equivalent to a system of four real equations for the variables $a_{10}^{(k)}$, $\varphi_{10}^{(k)}$ ($k = 1, 2$).

We introduce the notations

$$A = \Omega^{(+)},\ B = \mathrm{sign}(\gamma_2)\Omega^{(-)}\cos\delta_1,$$

$$C = -\mathrm{sign}(\gamma_2)\Omega^{(-)}\sin\delta_1,$$

$$X = \frac{A + |\gamma_1^{(1)}|C}{1 + (\gamma_1^{(1)})^2},\ Y = \frac{|\gamma_1^{(1)}|B}{1 + (\gamma_1^{(1)})^2},$$

$$Z = \frac{|\gamma_1^{(1)}|A - C}{1 + (\gamma_1^{(1)})^2},\ T = -\frac{B}{1 + (\gamma_1^{(1)})^2}.$$

Solving system (6), we have

$$a_{10}^{(1)} = a_{10}\sqrt{X^2 + Y^2},\ a_{10}^{(2)} = a_{10}\sqrt{Z^2 + T^2},$$

$$\delta_{x10}^{(1)} = \delta_{x10} + \mathrm{Arg}(X + \mathrm{i}Y),$$

$$\delta_{x10}^{(2)} = \delta_{x10} + \mathrm{Arg}(Z + \mathrm{i}T).$$

Using the described technique and taking into account formulae (3) and (4), we obtain the boundary conditions for normal modes:

$$a_{10}^{(1)} = 0.0720\mathrm{sech}[(w - 300)/50],\ \alpha_{10}^{(1)} = 0,$$
$$\gamma_{10}^{(1)} = 0.7417,\ \delta_{x10}^{(1)} = \delta_{x10} - 0.4993; \tag{7}$$

$$a_{10}^{(2)} = 0.1645\mathrm{sech}[(w - 300)/50],\ \alpha_{10}^{(2)} = \pi/2,$$
$$\gamma_{10}^{(2)} = -0.7417,\ \delta_{x10}^{(2)} = \delta_{x10} + 0.2884. \tag{8}$$

Note that on the input surface, the intensities of the normal modes have a bell-shaped shape, similar to that of the intensity of the total input probe field.

5. Results of numerical analysis

5.1. Phase modulation of probe radiation

We set in boundary conditions (3) and (4)

$$\delta_{x10} = 200\mathrm{sech}[(w - 300)/50],\quad \delta_{x20} = 0. \tag{9}$$

These conditions describe the situation when the input probe pulse is phase modulated with an instantaneous frequency deviation equal to Δ_1, and phase modulation of the control field is absent. (Below, the instantaneous frequency deviation will be called the modulus of the maximum displacement of the instantaneous frequency relative to the carrier frequency ω_1.)

Figure 1 shows the dependences of the quantities a_1, α_1 and γ_1 on the variable w for four values of the variable s. One can see that the input pulse of the total probe radiation decays in the medium into two fragments *1* and *2* with constant values of α_1 and γ_1 (see Figs 1c and 1d). The values of these quantities for fragment *1* coincide with the values inherent in the parallel normal mode, and for fragment *2* – with the values

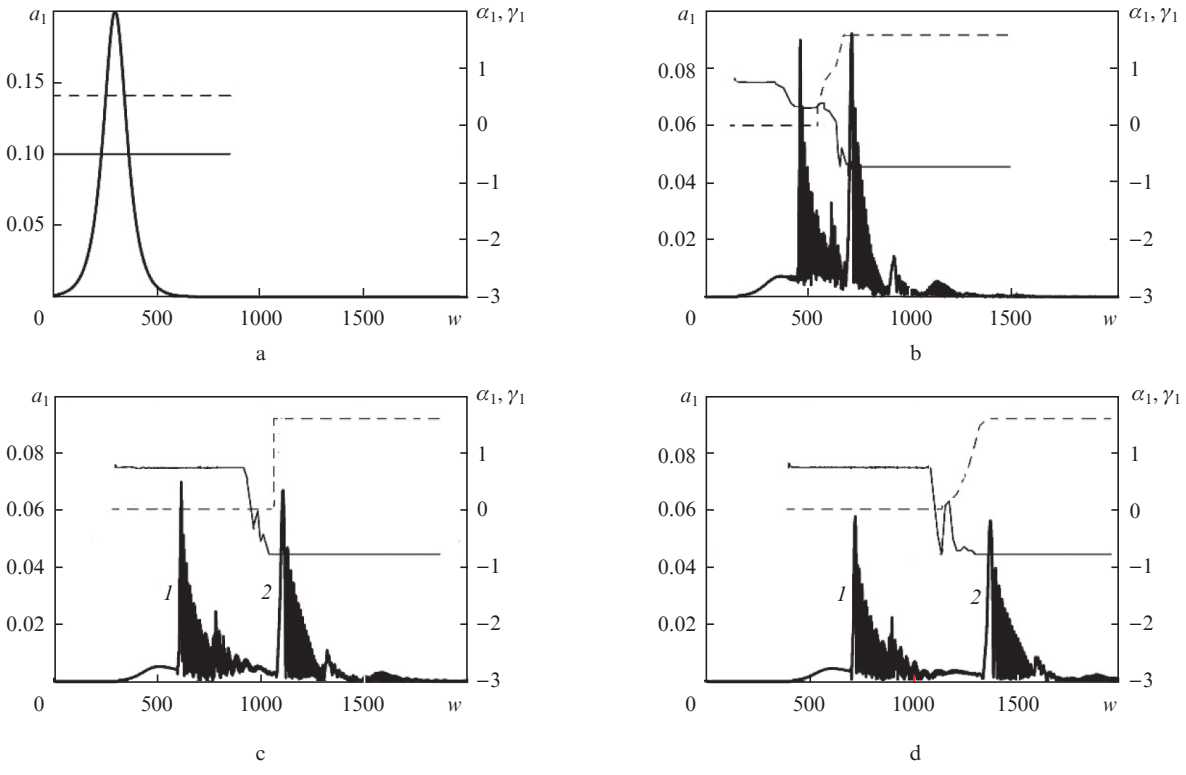

Figure 1. Evolution of the characteristics of the total probe field in a medium (a_1 = thick curves, α_1 = dashed lines, and γ_1 = thin lines) at s = (a) 0, (b) 1600, (c) 3000, and (d) 4000.

inherent in the perpendicular normal mode. The intensities $I_1^{(1)}$ and $I_1^{(2)}$, obtained by solving system (2) with boundary conditions (7) and (8), respectively, and the intensity I_1 of the total probe field, obtained by solving system (2) with boundary conditions (3) and (4), satisfy the condition $I_1 = I_1^{(1)} + I_2^{(2)}$ with an error less than 2% for all s and w. Hence it follows that fragments *1* and *2* are, respectively, parallel and perpendicular normal modes.

Fragments of normal modes at $s = 4000$ are shown in Fig. 2. Each mode is a train of subpulses with a duration in the range from 4 to 10 units of time w (from 0.6 to 1.6 ns, respectively). Note that the deviation of the instantaneous frequency in the region of each subpulse is approximately $0.07\Delta_1$. This is much less than the deviation of the instantaneous frequency of the total probe field at the resonant medium input.

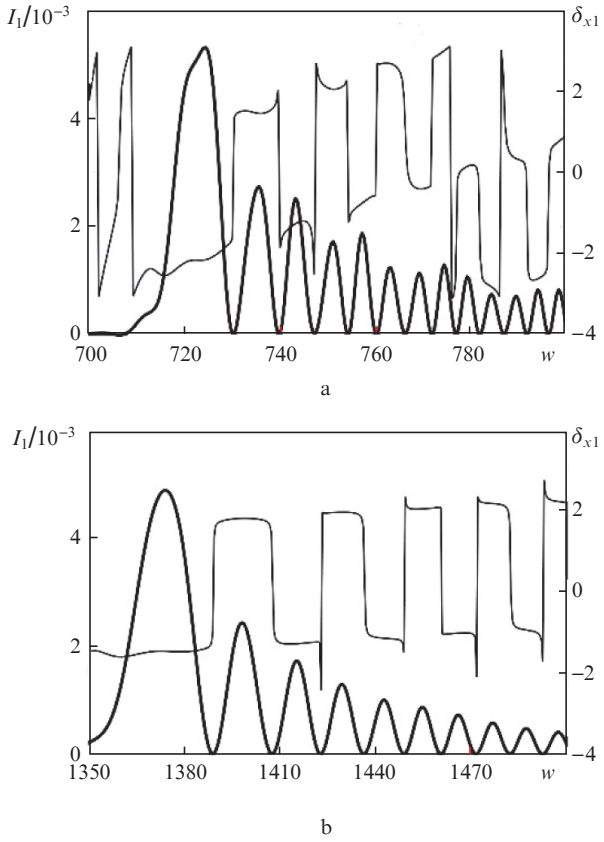

Figure 2. Evolution of the quantities I_1 (thick curves) and δ_{x1} (thin curves) at $s = 4000$ for (a) parallel and (b) perpendicular normal modes.

5.2. Pulsed phase modulation of control radiation

Below are the results of two calculations. In the first calculation it is assumed that

$$\delta_{x10} = 0, \quad \delta_{x20} = 200\mathrm{sech}[(w - 500)/50], \tag{10}$$

and in the second, it is assumed that

$$\delta_{x10} = 0, \quad \delta_{x20} = 200\mathrm{sech}[(w - 300)/50]. \tag{11}$$

Both calculations correspond to the case when the total input probe radiation has no phase modulation, and the phase modulation of the input control radiation is concentrated on a limited time interval, that is, has a pulsed character. Conditions (10) relate to the case when the pulse of the phase-modulated control radiation arrives at the input surface after the input probe pulse passed through this surface, catching up with it inside the medium. Conditions (11) describe the situation when the pulse of the phase-modulated control field crosses the input surface simultaneously with the pulse of the total probe radiation.

Figure 3 shows the calculated dependences of the characteristics a_1, α_1 and γ_1 on the variable w at $s = 1600$ and 4000 for boundary conditions (10) and (11). (The dependences of the quantities a_1, α_1 and γ_1 on w at $s = 0$ are shown in Fig. 1a.) According to Figs 3a and 3b, the bell-shaped input pulse of the total probe field in the medium splits into pulses of normal modes with bell-shaped envelopes a_1 and values of polarisation characteristics α_1 and γ_1 inherent in normal modes. This character of propagation of probe radiation in a medium is also realised in the absence of phase modulation of the interacting fields [25]. According to Figs 3c and 3d, the envelope has a multi-spike structure similar to that described in Section 5.1. The condition $I_1 = I_1^{(1)} + I_2^{(2)}$ is implemented with an error less than 2% in both calculations.

The dependences of the quantities I_1 and δ_{x1} for normal modes, obtained as a result of calculations with boundary conditions (10) at a distance of $s = 4000$, are shown in Fig. 4. The deviation of the instantaneous frequency of the parallel mode is approximately $0.13\Delta_1$, and that of the perpendicular mode is $0.05\Delta_1$, which is much less than the deviation of the instantaneous frequency of the control radiation, equal to Δ_1. Under boundary conditions (11), phase modulation of the normal modes of the probe field in the medium is close to that shown in Fig. 2.

Note that the control radiation propagates in the medium faster than normal mode pulses. Therefore, the pulse of the phase-modulated control radiation has practically no effect on the propagation of the probe radiation if it crosses the input surface before the probe radiation pulse arrives at it.

5.3. Continuous phase modulation of control radiation

Below are the results of calculations in which it is assumed that

$$\delta_{x10} = 0, \quad \delta_{x20} = 20\sin[(w - 300)/25]. \tag{12}$$

According to (12), the input probe radiation is not phase modulated, and phase modulation of the input control radiation has a periodic character with an instantaneous frequency deviation equal to $0.4\Delta_1$. Figure 5 shows the dependences of a_1, α_1 and γ_1 on the variable w for four values of the variable s. One can see that the input probe pulse splits in the medium into two separate pulses. The values of the polarisation characteristics of these pulses indicate that one of them (pulse *1* in Figs 5c and 5d) is a parallel pulse, and the other (pulse *2*) is a pulse of the perpendicular normal mode. This is confirmed by the fulfilment (with an error less than 2%) of the condition $I_1 = I_1^{(1)} + I_2^{(2)}$.

Fragments of normal modes at $s = 4000$ are shown in Fig. 6. Each mode is a train of subpulses with a duration in

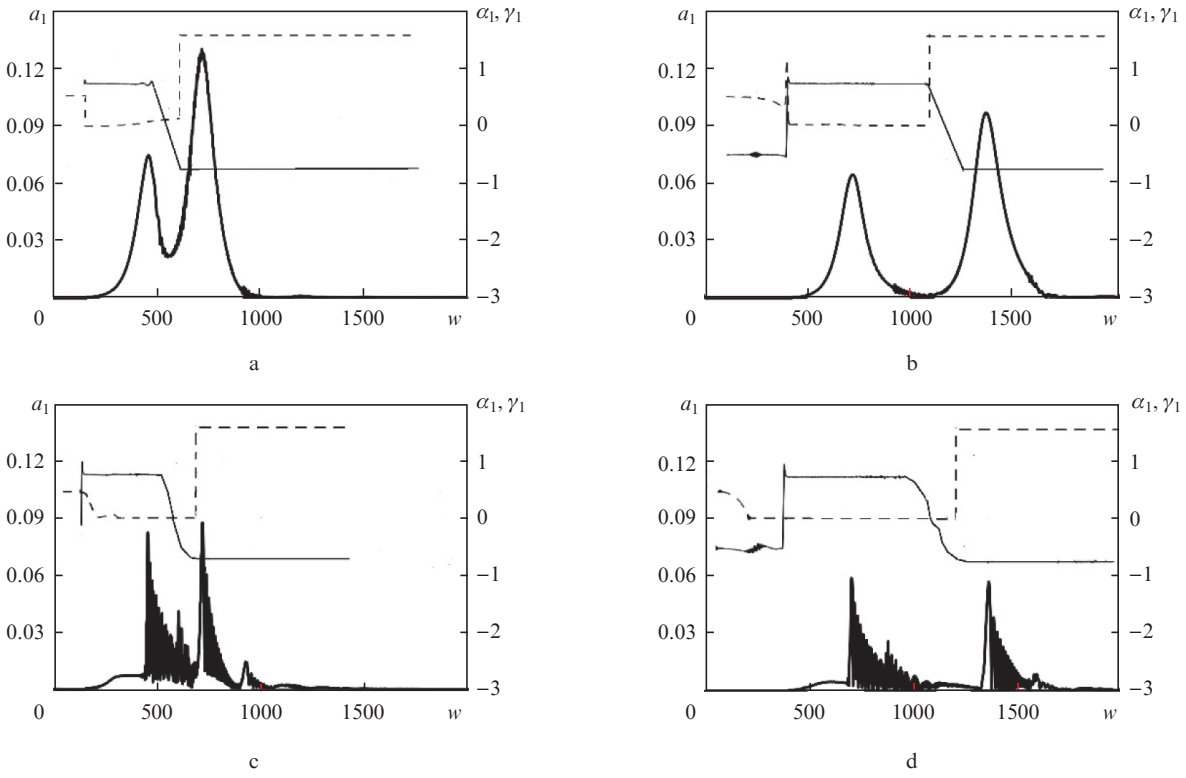

Figure 3. Evolution of the characteristics of the probe field in a medium (a_1 = thick curves, α_1 = dashed lines, and γ_1 = thin lines) under (a, b) boundary conditions (10) and (c, d) boundary conditions (11) at s = (a, c) 1600 and (b, d) 4000.

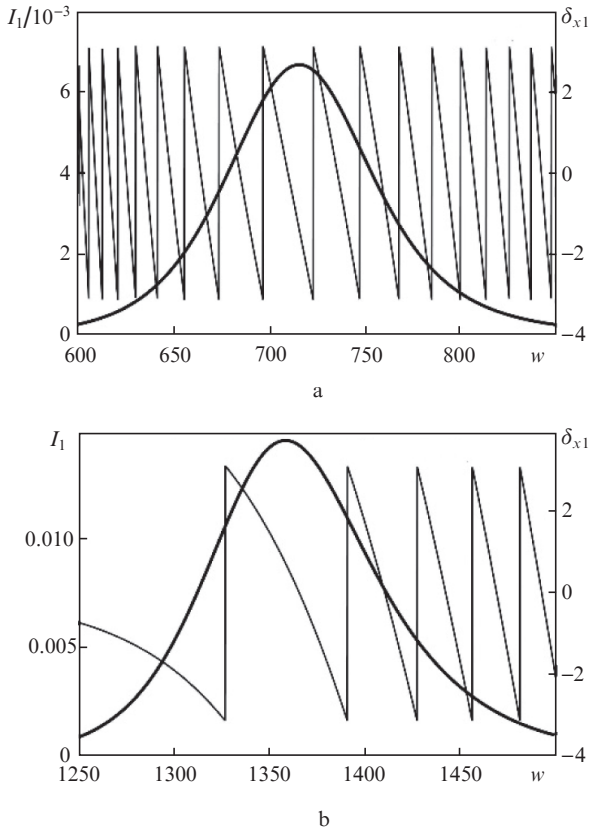

Figure 4. Evolution of the quantities I_1 (thick curves) and δ_{x1} (thin curves) at s = 4000 for (a) parallel and (b) perpendicular normal modes.

the range from 5 to 20 units of time w (from 0.8 to 3 ns, respectively). In the region of the most intense subpulses, the deviation of the instantaneous frequency is about $0.25\Delta_1$ for the parallel normal mode and $0.7\Delta_1$ for the perpendicular normal mode.

5.4. Normal mode velocities

The values of the group velocities of propagation of normal modes differ insignificantly when passing from one calculation to another. With an error less than 3%, we can assume that $V_1^{(1)} = 9.5$, while $V_1^{(2)} = 3.7$, where $V_1^{(k)}$ are the velocities of the parallel ($k = 1$) and perpendicular ($k = 2$) modes in the reference frame w, s. At $T_{\mathrm{Pb}} = 950$ K, we find that if $v_1^{(1)}$ and $v_1^{(2)}$ are the velocities of pulses of parallel and perpendicular normal modes in a stationary frame of reference z, t, and c is the speed of light in a vacuum, then $c/v_1^{(1)} \approx 16$, while $c/v_1^{(2)} \approx 40$. According to the calculations given in [25], in the absence of phase-modulated input radiation, the normal mode pulse velocities have almost the same values.

5.5. Transparency of the medium

Let us define the transparency of the medium for the probe field as $Tr = W(s)/W(0)$, where $W(s)$ is the amount of energy transferred by the probe radiation through a unit cross-sectional area located at a distance s from the input surface for the entire time of radiation propagation through this section. The Tr value is an important characteristic of the efficiency of the EIT phenomenon.

Calculations have shown that in all cases the Tr value for the parallel normal mode is greater than that for the perpendicular normal mode. The largest Tr values are obtained by in

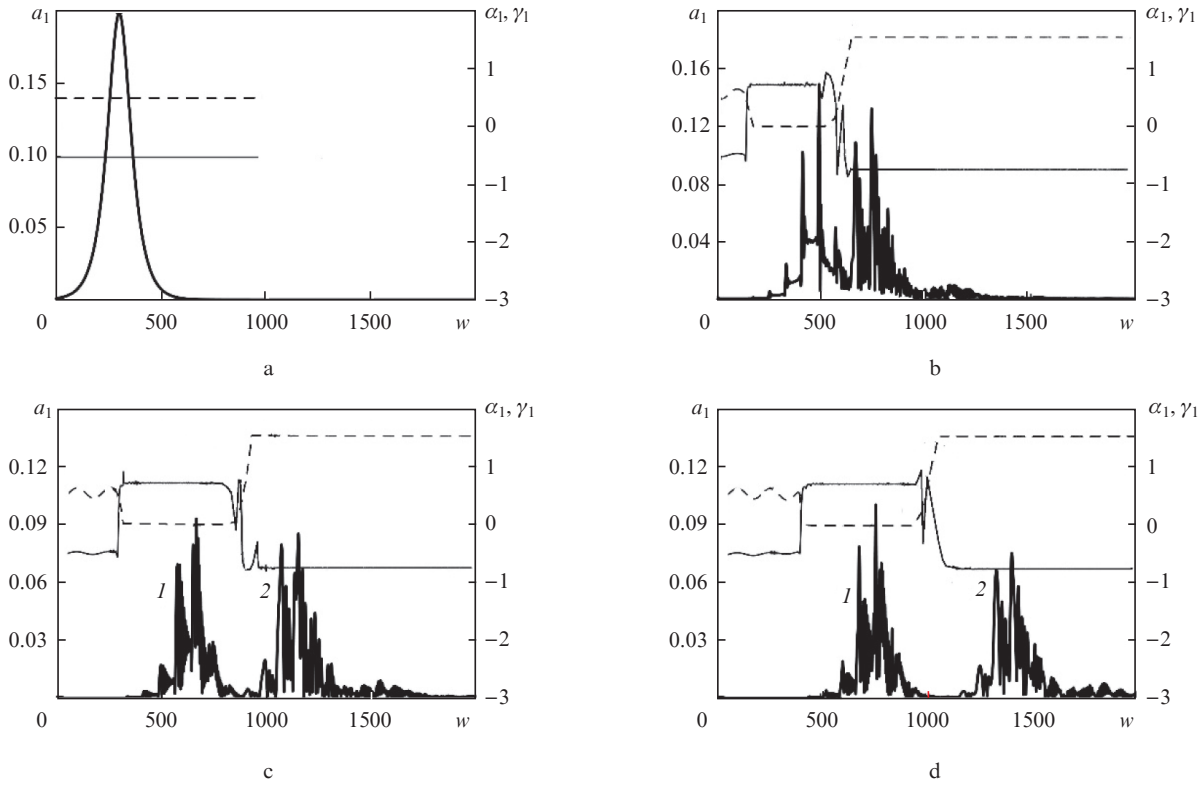

Figure 5. Evolution of the characteristics of the total probe field in a medium (a_1 = thick curves, α_1 = dashed lines, and γ_1 = thin lines) at s = (a) 0, (b) 1500, (c) 3000, and (d) 4000.

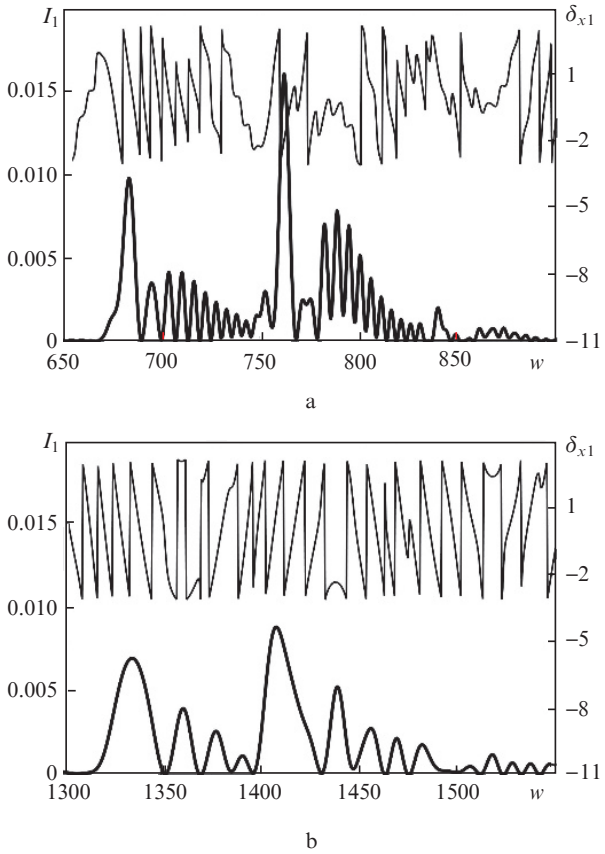

Figure 6. Evolution of the quantities I_1 (thick curves) and δ_{x1} (thin curves) at s = 4000 for (a) parallel (a) and (b) perpendicular normal modes.

calculations with boundary conditions (10), which mean that the pulse of the phase-modulated control field on the input surface lags in time from the pulse of the probe field. In this case, for $s = 4000$, the Tr values are 0.86 and 0.41 for the parallel and perpendicular normal modes, respectively, and 0.48 for the total probe field consisting of emissions from these modes.

The smallest Tr value was recorded in calculations with initial conditions (9). The corresponding dependences of Tr on s for the total field and fields of normal modes are shown in Fig. 7 by thick curves. For comparison, an additional calculation was carried out, in which instead of condition (9) it was assumed that $\delta_{x10} = \delta_{x20} = 0$, that is, it was assumed that both input fields exhibited no phase modulation (thin curves in Fig. 7). One can see that the presence of phase modulation of the input probe field significantly reduces the EIT efficiency.

Another additional calculation proceeded from conditions (9), but instead of the value $a_{20} = 6.65$ in conditions (4), it was assumed that $a_{20} = 0$. This corresponds to the absence of control radiation, that is, to the absence of the EIT phenomenon. This calculation showed that $Tr < 10^{-3}$ at $s = 100$; at the same distance, the transparency of the medium for the parallel and perpendicular normal modes is 0.56 and 0.22, respectively. Hence, we can conclude that in the presence of the phase-modulated input probe radiation the EIT phenomenon occurs quite efficiently. This conclusion remains valid for all calculations presented in this work.

6. Conclusions

The obtained results indicate that even with a significant phase modulation of the input probe radiation (the deviation

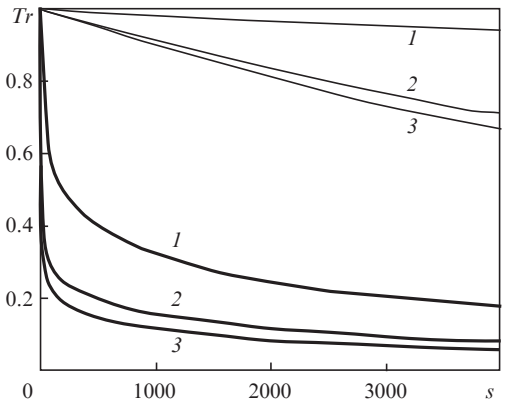

Figure 7. Dependences of the medium transparency *Tr* on *s* in the presence of phase modulation of the input probe radiation (thick curves) and in its absence (thin curves) for (*1*) parallel and (*3*) perpendicular normal modes as well as for (*2*) total radiation.

of the instantaneous frequency is equal to the inhomogeneous width Δ_1 of the transition line resonant to this radiation), the probe field in the medium is the sum of normal modes propagating independently of each other. If a total probe field at the medium input is represented by a bell-shaped pulse, then on the input surface the normal modes have the same shape. However, inside the medium, each normal mode takes the form of a train of short subpulses. In this case, phase modulation of each subpulse is small: the maximum deviation of the instantaneous frequency is less than $0.1\Delta_1$.

The mode structure of the probe field in the medium is retained even in the presence of phase-modulated control radiation. If phase modulation of the control field is concentrated on a limited time interval that does not overlap with the time the probe pulse crosses the input surface of the medium, then it insignificantly affects the EIT process: the mode pulses in the medium have a bell-shaped shape and an insignificant phase modulation. (The bell-shaped structure of the envelopes is inherent in modes in the absence of phase modulation of the interacting fields.) However, if the pulse of the phase-modulated control field and the input probe pulse pass through the input surface simultaneously, the normal modes inside the medium have a multi-spike structure similar to that described above. Continuous phase modulation of the control field also leads to a multi-spike structure of normal modes.

The presence of phase-modulated interacting fields significantly reduces the transparency of the medium for probe radiation, except for the case when the pulse of the phase-modulated control field on the input surface does not overlap in time with the pulse of the input probe radiation. However, the influence of the phase-modulated input fields on the propagation velocity of normal modes is insignificant in all cases.

The results of this work can be used in the development and improvement of devices based on the EIT phenomenon of pulsed probe radiation, for example, optical memory [3], quantum communications [3, 5, 6] and quantum information systems [2–4].

References

1. Demtröder W. *Laser Spectroscopy: Basic Concepts and Instrumentation* (Berlin: Springer, 2002; Dolgoprudnyi: ID 'Intellekt', 2014).
2. Harris S.E. *Phys. Today*, **50**, 36 (1997).
3. Lukin M.D. *Rev. Mod. Phys*., **75**, 457 (2003).
4. Fleischhauer M., Imamoğlu A., Marangos J.P. *Rev. Mod. Phys*., **77**, 633 (2005).
5. Duan L.-M., Lukin M.D., Cirac J.I., Zoller P. *Nature* (*London*), **414**, 413 (2001).
6. Sinatra A. *Phys. Rev. Lett*., **97**, 253601 (2006).
7. Martinalli M., Valente P., Failache H., Felinto D., Cruz L.S., Nussenzveig P., Lezama A. *Phys. Rev. A*, **69**, 043809 (2004).
8. Godone A., Micallilizio S., Levi F. *Phys. Rev. A*, **66**, 063807 (2002).
9. Lukin M.D., Imamoğlu A. *Nature* (*London*), **413**, 273 (2001).
10. Kocharovskaya O., Mandel P. *Phys. Rev. A*, **42**, 523 (1990).
11. Jen H.H., Daw-Wei Wang. *Phys. Rev. A*, **87**, 061802(R) (2013).
12. Basler C., Grzesiak J., Helm H. *Phys. Rev. A*, **92**, 013809 (2015).
13. Liu R., Liu T., Wang Y., Li Y., Gai B. *Phys. Rev. A*, **96**, 053823 (2017).
14. Le Kien F., Rauschenbeutel A. *Phys. Rev. A*, **91**, 053847 (2015).
15. Wang H.-H., Wang J., Kang Z.-H., Wang L., Gao J.-Y., Chen Y., Zhang X.-J. *Phys. Rev. A*, **100**, 013822 (2019).
16. Wielandy S., Gaeta A.L. *Phys Rev. Lett*., **81**, 3359 (1998).
17. Wang B., Li S., Ma J., Wang H., Peng K.C., Xiao M. *Phys. Rev. A*, **73**, 051801(R) (2006).
18. Agarwal G.S., Dosgupta S. *Phys. Rev. A*, **67**, 023814 (2003).
19. Sautenkov V.A., Rostovtsev Y.V., Chen H., Hsu P., Agarwal G.S., Scully M.O. *Phys. Rev. Lett*., **94**, 233601 (2005).
20. Yoon T.H., Park C.Y., Park S.J. *Phys. Rev. A*, **70**, 061803(R) (2004).
21. Kis Z., Demeter G., Janszky J.J. *Opt. Soc. Am. B*, **30**, 829 (2013).
22. Grobe R., Hioe F.T., Eberly J.H. *Phys. Rev. Lett*., **73**, 3183 (1994).
23. Shakhmuratov R.N., Odeurs J. *Phys. Rev. A*, **74**, 043807 (2006).
24. Kozlov V.V., Kozlova E.B. *Opt. Commun.,* **282** (5), 892 (2009).
25. Parshkov O.M. *Quantum Electron*., **48** (11), 1027 (2018) [*Kvantovaya Elektron*., **48** (11), 1027 (2018)].
26. Kasapi A., Jain M., Yin G.Y., Harris S.E. *Phys. Rev. Lett*., **74** (13), 2447 (1995).
27. Jain M., Kasapi A., Yin G.Y., Harris S.E. *Phys. Rev. Lett*., **75** (24), 4385 (1995).
28. Saleh B.E.A., Teich M.C. *Fundamentals of Photonics* (Hoboken N.J.: Wiley-Interscience, 2007) Vol. 1.
29. Parshkov O.M. *Quantum Electron*., **47** (10), 892 (2017) [*Kvantovaya Elektron*., **47** (10), 892 (2017)].